RSC Advances

PAPER

View Article Online
View Journal | View Issue

Cite this: *RSC Adv.*, 2017, **7**, 22301

Tuning of luminescence properties by controlling an aid-sintering additive and composition in Na(Ba/Sr/Ca)PO_4:Eu^{2+} for white LEDs

Qiongyu Bai, Panlai Li,* Zhijun Wang,* Shuchao Xu, Ting Li and Zhiping Yang

Received 27th March 2017
Accepted 5th April 2017

DOI: 10.1039/c7ra03557h

rsc.li/rsc-advances

A series of Na(Ba/Sr/Ca)PO_4:Eu^{2+} phosphors were prepared *via* a high-temperature solid-state reaction method. When the phase of $NaCaPO_4$:Eu^{2+} was pure, the luminescence of Eu^{2+} was enhanced by doping the sintering-aid additive NaCl (*t*), and it showed a maxima at $t = 0.03$. For $NaCaPO_4$:Eu^{2+} with 0.03NaCl, the XRD patterns, and emission and decay spectra demonstrated that Eu^{2+} ions occupied two different Ca sites with different coordination (*i.e.*, eight and seven coordination). Therefore, two green emission bands at 510 and 542 nm were observed, and the emission band ranging from 480 to 510 nm had a weaker intensity. To obtain a cyan-broad emission, Ba^{2+} or Sr^{2+} were introduced into $NaCaPO_4$:$0.01Eu^{2+}$. The substitution of small Ca^{2+} ions by large Ba^{2+} or Sr^{2+} ions induced a decreased crystal field splitting of Eu^{2+} ions, which resulted in various full width at half maximum and a blue shift. The colors varied from green (0.1996, 0.4380) to blue (0.1578, 0.0978) under the same excitation. Overall, the phosphor has promising applications for use in white LEDs.

1 Introduction

Nowadays, white light-emitting diodes (LED) have attracted significant attention as next generation lighting devices due to their advantages of energy saving and long lifetime.[1–7] To date, most commercial white LEDs have been fabricated *via* a combination of blue LED chips and yellow emitting $Y_3Al_5O_{12}$:Ce^{3+} phosphors. However, these white LEDs exhibit a low color rendering index (<75) and a high correlated color temperature (~7750 K) due to the lack of a red component.[8–12] Today, the most effective method to obtain white light is to combine an ultraviolet (UV) LED chip with tricolor phosphors.[13–16] However, it usually shows lower luminescence efficiency due to strong reabsorption. Moreover, it shows lower color vividness because the cyan component in the range of 480–520 nm is weaker.[17] Therefore, it is necessary to develop a cyan phosphor with a broad emission band that has strong absorption in the near-UV but at the same time has no absorption in the visible region.[18]

Phosphate hosts with the chemical formula $ABPO_4$ (where A and B are the alkali and alkaline earth cations, respectively) are good candidates as hosts due to their several advantages such as they require low synthesis temperature and have high chemical and physical stability; moreover, they exhibit excellent luminescence properties when Eu^{2+} is doped as an activator, such as $LiSrPO_4$ and $KSrPO_4$.[19–25] In our previous study, a green-emitting $NaCaPO_4$:Eu^{2+} phosphor was synthesized, which can be used in a white LED.[26] After this, green emission was enhanced in $NaCaPO_4$:Eu^{2+}, Tb^{3+} *via* energy transfer, according to Wang *et al.*[27] In our study, to avoid a decreased luminescence efficiency due to energy transfer and save energy, the green emission of Eu^{2+} ions was enhanced by doping NaCl as an aid-sintering additive in $NaCaPO_4$. Hence, a series of $NaCaPO_4$:Eu^{2+} phosphors was synthesized by a high temperature solid-state method. They showed a green emission band at 515 nm; however, the emission band ranging from 480 to 510 nm was weaker. Therefore, to adjust the emission band and enhance the emission band in the range of 480–510 nm, Ba^{2+} or Sr^{2+} ions with larger radii were introduced in $NaCaPO_4$:Eu^{2+} with 0.03NaCl. The emission band showed an obvious blue shift, and the color ranged from green to blue with the increasing concentrations of Ba^{2+} or Sr^{2+} ions; thus, these phosphors can be used in white LEDs.

2 Experimental

2.1 Sample preparation

A series of phosphors with the composition $NaCaPO_4$:xEu^{2+} with *t*NaCl ($t = 0.01$–0.05 mol and $x = 0.001$–0.10 mol), Na(Ba_aCa_b)PO_4:$0.01Eu^{2+}$ with 0.03NaCl and Na(Sr_cCa_d)PO_4:$0.01Eu^{2+}$ with 0.03NaCl were synthesized by a high temperature solid state method using reagent grade $CaCO_3$, $BaCO_3$, $SrCO_3$, NaCl, Na_2CO_3, $NH_4H_2PO_4$, and Eu_2O_3 (99.99%) as raw materials. Starting materials were weighed according to stoichiometric proportion, thoroughly mixed, and ground using an agate mortar and pestle for more than 30 min until they were

Hebei Key Lab of Optic-electronic Information and Materials, College of Physics Science & Technology, Hebei University, Baoding 071002, China. E-mail: li_panlai@126.com; wangzj1998@126.com

uniformly distributed. The obtained mixtures were heated at 1200 °C for 2 h in the reduction environment (95% H^2 + 5% N^2) and then naturally cooled down to room temperature to obtain the final phosphors.

2.2 Characterization

A Bruker D8 X-ray diffractometer was utilized to examine the X-ray powder diffraction (XRD) with Ni-filtered Cu Kα radiation (λ = 0.15418 nm), operating at 40 mA and 40 kV. The step length and diffraction range were 0.05° and 10–80°, respectively. To analyze the chemical composition of the phosphors, scanning electron microscopy (SEM) images and electron-dispersive X-ray (EDX) data were obtained by a Nova NanoSEM 650 with the accelerating voltage of 10 kV. Room temperature photoluminescence spectra of the samples were obtained *via* a Hitachi F-4600 fluorescence spectrophotometer using a 450 W Xe lamp as the excitation source, with the scanning wavelength ranging from 200 to 700 nm, scanning at 240 nm min^{-1}. The temperature-dependent luminescent properties were obtained using a computer-controlled electric furnace and a self-made heating attachment. Luminescence decay curves and quantum efficiencies of the samples were obtained using a Horiba FL-4600 fluorescence spectrophotometer. Herein, to obtain the luminescence decay curves, a nano-LED (370 nm) was used as the excitation source. The Commission International de l'Eclairage (CIE) coordinates for all samples were measured by a PMS-80 UV-VIS NEAR IR spectra analysis system.

3 Results and discussion

3.1 $NaCaPO_4$:0.01Eu^{2+} with *t*NaCl

$NaCaPO_4$:Eu^{2+} showed a broad emission band at 505 nm, according to our previous study.[26] However, it showed weaker luminescence intensity. Hence, we introduced NaCl as an aid-sintering additive to enhance the emission intensity. To verify the influence of NaCl on the emission intensity, the concentration of Eu^{2+} was randomly fixed at 0.01 mol. Fig. 1 shows the XRD patterns of $NaCaPO_4$:0.01Eu^{2+} and $NaCaPO_4$:0.01Eu^{2+} with *t*NaCl (*t* = 0.01, 0.02, 0.03, 0.04, and 0.05). It can be seen that the XRD patterns of $NaCaPO_4$:0.01Eu^{2+} with *t*NaCl are indexed to $NaCaPO_4$ (JCPDS no. 29-1193) and no impurity phase was detected, indicating that NaCl has no influence on the phase of the phosphor. To further investigate the influence of NaCl on the phase of the phosphor, the crystal structure of $NaCaPO_4$:0.01Eu^{2+} with 0.03NaCl sample was refined using the General Structure Analysis System (GSAS) program.[28] Fig. 2 shows the XRD pattern for Rietveld structure analysis of $NaCaPO_4$:0.01Eu^{2+} with 0.03NaCl based on the $NaCaPO_4$ phase model, and no impurity phase was detected. The final profile *R*-factors, R_{wp}, R_p, and χ^2 obtained were 8.62%, 6.19% and 1.539, respectively, which suggested that the pure $NaCaPO_4$:0.01Eu^{2+} with 0.03NaCl was successfully synthesized. $NaCaPO_4$ was indexed to an orthorhombic crystal system and space group *Pnam* (a = 0.6797 nm, b = 0.9165 nm, c = 0.5406 nm, and V = 0.3368 nm^3). The cell parameters and volume of $NaCaPO_4$:0.01Eu^{2+} with 0.03NaCl were a = 0.680 nm, b = 0.916 nm, c = 0.542 nm, and V = 0.3376 nm^3, which are larger than those of $NaCaPO_4$, indicating that Eu^{2+} was doped into the host. The crystal structure of $NaCaPO_4$ viewed down the *b*-axis and the coordination polyhedron was composed of a Na/Ca/P atomic site, as shown in Fig. 2. A total of three independent Na and Ca cation polyhedral sites were available with the coordination number ranging from 6 to 8 in the unit cell of $NaCaPO_4$. Fig. 2 shows the presence of three different crystallographic Na environments: seven-coordinated Na(1) atom with

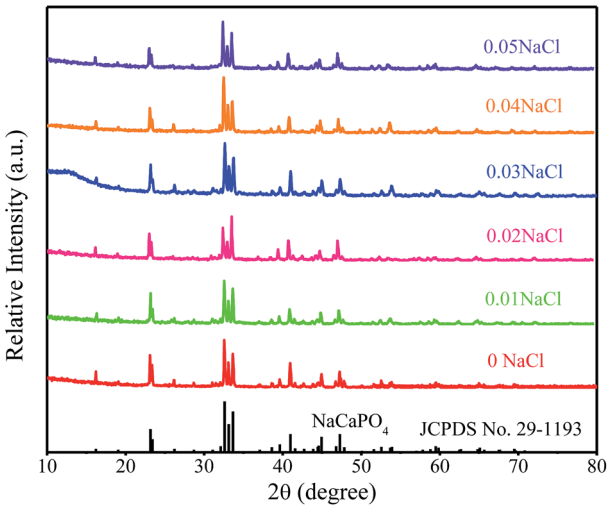

Fig. 1 XRD patterns of $NaCaPO_4$:0.01Eu^{2+} and $NaCaPO_4$:0.01Eu^{2+} with *t*NaCl (*t* = 0.01, 0.02, 0.03, 0.04, and 0.05). The standard data for $NaCaPO_4$ (JCPDS no. 29-1193) are shown as a reference.

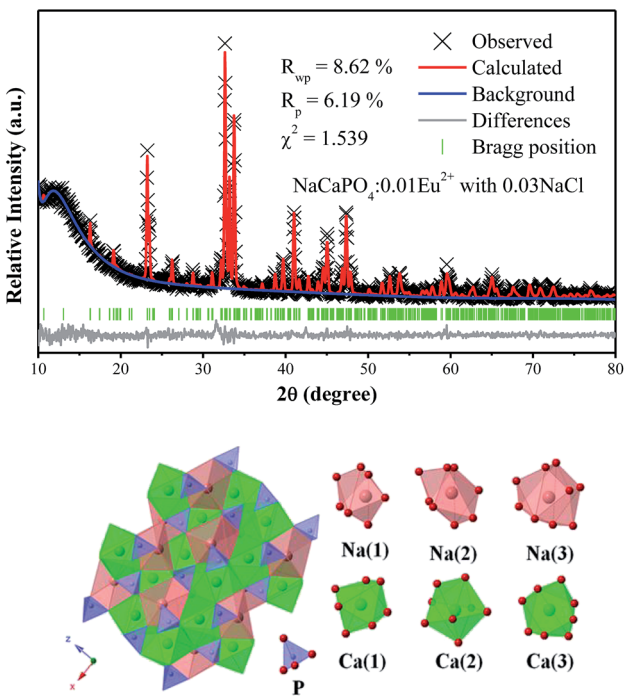

Fig. 2 XRD Rietveld refinement result of $NaCaPO_4$:0.01Eu^{2+} with 0.03NaCl, and the crystal structure of $NaCaPO_4$.

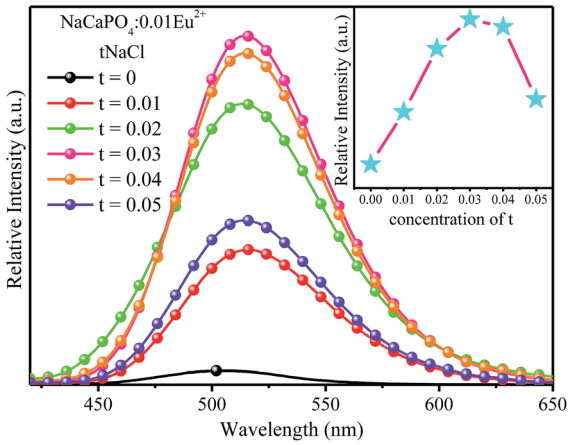

Fig. 3 Emission spectra of $NaCaPO_4$:0.01Eu^{2+} and $NaCaPO_4$:0.01-Eu^{2+} with *t*NaCl (t = 0.01, 0.02, 0.03, 0.04, and 0.05) excited at 365 nm. The inset shows the emission intensity at 515 nm depending on t concentration.

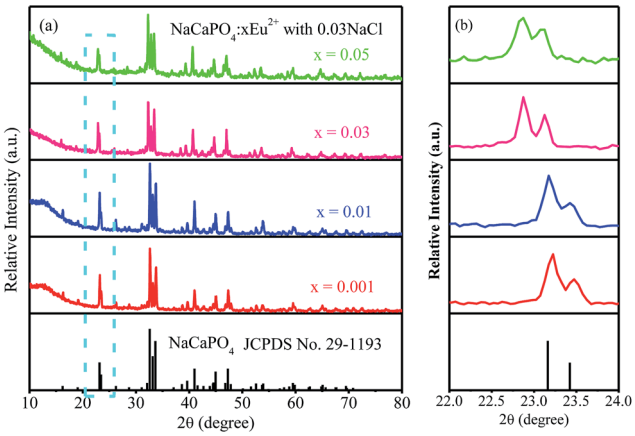

Fig. 4 XRD patterns (a) and magnified patterns between 22° and 24° (b) of $NaCaPO_4$:xEu^{2+} with 0.03NaCl (x = 0.001, 0.01, 0.03, and 0.05). The standard data for $NaCaPO_4$ (JCPDS no. 29-1193) are shown as a reference.

an average Na(1)–O distance of 0.260 nm, Na(2) atom surrounded by eight O atoms at the average distances of 0.264 nm, and a Na(3) atom that was nine-coordinated by nine O atoms at the average Na(3)–O distance of 0.268 nm. There were three crystallographic positions of Ca in the unit cell: seven-coordinated Ca^{2+} sites (Ca(1)) with the average Ca–O distance of 0.244 nm and two eight-coordinated Ca^{2+} sites (Ca(2)/Ca(3)) with the average Ca–O distance of 0.246 nm and 0.249 nm, respectively. P atoms with four-coordination modes could also be observed.

Fig. 3 shows the emission spectra of $NaCaPO_4$:0.01Eu^{2+} and $NaCaPO_4$:0.01Eu^{2+} with *t*NaCl (t = 0.01, 0.02, 0.03, 0.04, and 0.05) excited at 365 nm. They exhibited a green emission band ranging from 400 to 600 nm. The intensity of $NaCaPO_4$:0.01Eu^{2+} with *t*NaCl increased with the increase in Eu^{2+} ions, reached a maximum at t = 0.03, and then decreased (inset of Fig. 3). Compared to $NaCaPO_4$:0.01Eu^{2+}, the intensity of $NaCaPO_4$:0.01Eu^{2+} with 0.03NaCl was 10 times enhanced. Therefore, to further investigate the influence of doping concentration on luminescence and improve the luminescent properties, a series of Na(Ba/Sr/Ca)PO4:Eu^{2+} with 0.03NaCl was synthesized.

3.2 Na(Ba/Sr/Ca)PO_4:Eu^{2+} with 0.03NaCl

3.2.1 Phase formation and structure. The XRD patterns and the magnified patterns between 22° and 24° of $NaCaPO_4$:-xEu^{2+} with 0.03NaCl with x = 0.001, 0.01, 0.03, and 0.05 are shown in Fig. 4a and b, respectively. It can be seen that all the peaks could be indexed to standard JCPDS no. 29-1193, suggesting that the phosphors are high-purity. According to the effective ionic radii of cations, Eu^{2+} ions were proposed to occupy the Ca^{2+} sites in $NaCaPO_4$. The ionic radii for the seven- and eight-coordinated Ca^{2+} ions were 0.106 and 0.112 nm, respectively; thus, the Ca^{2+} sites in $NaCaPO_4$ may be occupied by Eu^{2+} ions with similar ionic radii of 0.121 and 0.125 nm for the same coordination, respectively. The diffraction peaks of

Table 1 Cell parameters and volumes of $NaCaPO_4$:xEu^{2+} with 0.03NaCl

	Cell parameters			Volumes
Formula	a (nm)	b (nm)	c (nm)	V (nm^3)
$NaCaPO_4$:0.001Eu^{2+}	0.6798	0.9158	0.5412	0.3369
$NaCaPO_4$:0.01Eu^{2+}	0.6800	0.9160	0.5420	0.3376
$NaCaPO_4$:0.03Eu^{2+}	0.6810	0.9168	0.5430	0.3390
$NaCaPO_4$:0.05Eu^{2+}	0.6815	0.9169	0.5464	0.3414

$NaCaPO_4$:xEu^{2+} with 0.03NaCl slightly shifted to a lower angle, and it can be seen from Table 1 that the unit cell expanded with the increasing Eu^{2+} concentration. Because the radius of Ca^{2+} is

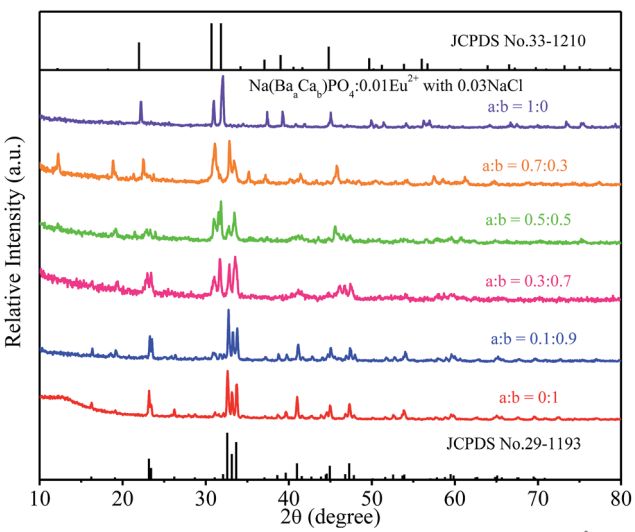

Fig. 5 XRD patterns of Na(Ba_aCa_b)PO_4:0.01Eu^{2+} with 0.03NaCl and standard data (JCPDS no. 29-1193 and JCPDS no. 33-1210).

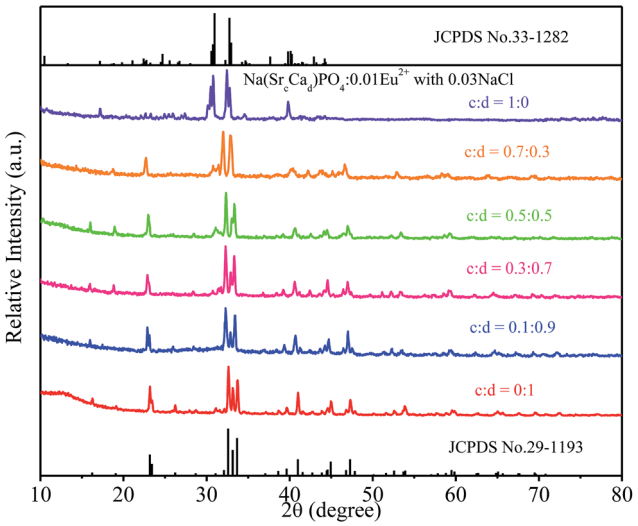

Fig. 6 XRD patterns of Na(Sr$_c$Ca$_d$)PO$_4$:0.01Eu^{2+} with 0.03NaCl and standard data (JCPDS no. 29-1193 and JCPDS no. 33-1282).

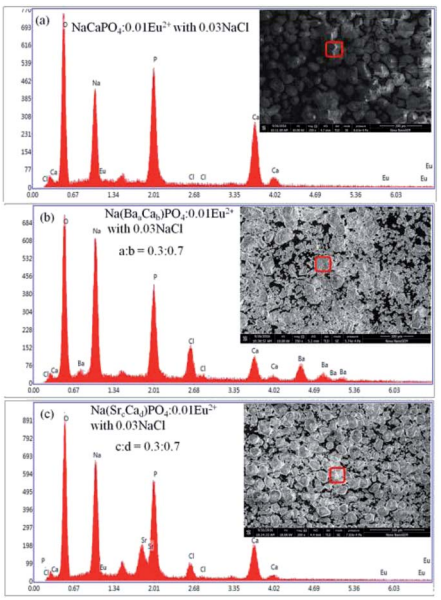

Fig. 7 SEM images and EDX spectra of NaCaPO$_4$:0.01Eu^{2+} with 0.03NaCl, Na(Ba$_a$Ca$_b$)PO$_4$:0.01Eu^{2+} with 0.03NaCl ($a : b = 0.3 : 0.7$) and Na(Sr$_c$Ca$_d$)PO$_4$:0.01Eu^{2+} with 0.03NaCl ($c : d = 0.3 : 0.7$).

slightly smaller than that of Eu^{2+}, Eu^{2+} can be easily doped into the host lattice and substituted for the site of Ca^{2+} ions.

XRD patterns of Na(Ba$_a$Ca$_b$)PO$_4$:0.01Eu^{2+} with 0.03NaCl ($a : b$ = 0 : 1, 0.1 : 0.9, 0.3 : 0.7, 0.5 : 0.5, 0.7 : 0.3, and 1 : 0) phosphors are given in Fig. 5. The standard data for NaCaPO$_4$ (JCPDS no. 29-1193) and NaBaPO$_4$ (JCPDS no. 33-1210) are also shown as a reference in Fig. 5. We can see that Na(Ba$_a$Ca$_b$)PO$_4$:0.01Eu^{2+} with 0.03NaCl can be basically indexed to the NaCaPO$_4$ phase (JCPDS no. 29-1193) when $a \leq 0.5$. The phases of Na(Ba$_a$Ca$_b$)PO$_4$:0.01Eu^{2+} with 0.03NaCl agreed well with the standard data for the NaBaPO$_4$ phase (JCPDS no. 33-1210) with the increase of a.

To further investigate the phase formation depending on the Sr/Ca substitution of Na(Sr$_c$Ca$_d$)PO$_4$:0.01Eu^{2+} with 0.03NaCl phosphors, XRD patterns for the selected samples were obtained and are shown in Fig. 6. All the diffraction peaks of the selected samples agreed well with the standard data for the NaCaPO$_4$ phase (JCPDS no. 29-1193) and NaSrPO$_4$ phase (JCPDS no. 33-1282), indicating that Eu^{2+} ions were successfully incorporated in the host without noticeably changing the crystal structure.

Fig. 7a–c shows the representative SEM images and EDX spectra of NaCaPO$_4$:0.01Eu^{2+} with 0.03NaCl, Na(Ba$_a$Ca$_b$)PO$_4$:0.01Eu^{2+} with 0.03NaCl ($a : b = 0.3 : 0.7$) and Na(Sr$_c$Ca$_d$)PO$_4$:0.01Eu^{2+} with 0.03NaCl ($c : d = 0.3 : 0.7$). It can be clearly observed that the grains of NaCaPO$_4$:0.01Eu^{2+} with 0.03NaCl have a spherical shape, and the EDX results indicates that the phosphor has a chemical composition of Na, Ca, P, O, Cl, and Eu. Phosphors showed an irregular shape of blocky particles when Ba^{2+} and Sr^{2+} were doped in NaCaPO$_4$:0.01Eu^{2+} with 0.03NaCl. The EDX spectra of Na(Ba$_a$Ca$_b$)PO$_4$:0.01Eu^{2+} with 0.03NaCl ($a : b = 0.3 : 0.7$) and Na(Sr$_c$Ca$_d$)PO$_4$:0.01Eu^{2+} with 0.03NaCl ($c : d = 0.3 : 0.7$) confirmed the presence of all elements in the samples. These results suggest that well-crystallized powders were obtained.

3.2.2 Luminescence properties

3.2.2.1 NaCaPO$_4$:xEu^{2+} with 0.03NaCl. Fig. 8a–f show the emission spectra of NaCaPO$_4$:xEu^{2+} with 0.03NaCl (x = 0.001, 0.01, 0.03, 0.05, 0.07, and 0.10) excited at 365 nm, respectively. We fitted the emission spectra with a Gaussian function for NaCaPO$_4$:xEu^{2+} with 0.03NaCl. The orange dashed lines denote two Gaussian functions, which successfully fitted with the maxima at 510 (Eu2) and 542 (Eu1) nm. Moreover, two different emission bands were obtained due to the different crystal surroundings of Eu^{2+} sites. From the XRD patterns and structural analysis, it can be inferred that Eu^{2+} ions occupied Ca^{2+} sites in NaCaPO$_4$. Hence, three distinct crystallographic sites were formed (*i.e.*, Ca(1), Ca(2), and Ca(3), in which both the crystallographic sites of Ca(2) and Ca(3) were eight-coordinated).

Therefore, the emission spectra were fitted by two Gaussian curves, and due to this, the luminescence of the luminescence centers with similar coordinate environments was indistinguishable, according to crystal field theory.[29] In addition, to investigate the relationship between the coordinate environment and emission peaks, the emission position of Eu^{2+} can be simply estimated using the Van Uitert eqn (1):[30,31]

$$E = Q\left[1 - \left(\frac{V}{4}\right)^{\frac{1}{V}} \times 10^{\frac{nE_a r}{80}}\right] \quad (1)$$

where E is the energy location of the lower d-band edge for Eu^{2+} (cm^{-1}), Q is the energy location for the lower d-band edge of the free ion (Q = 34 000 cm^{-1} for Eu^{2+}), V is the valence of the active cation (V = 2 for Eu^{2+}), n is the coordination number, and r is the radius of the host cation (Ca^{2+}) replaced by the activator Eu^{2+} ion (Å). The value of E_a was difficult to obtain due to the complexity of the host, but it was constant in the same host. E is

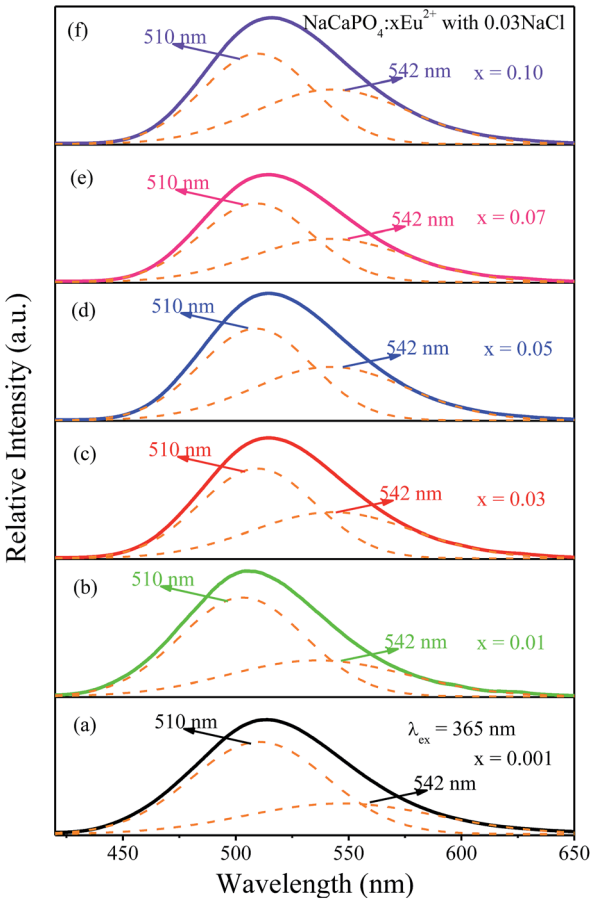

Fig. 8 Emission spectra of $NaCaPO_4$:xEu^{2+} with 0.03NaCl (x = 0.001, 0.01, 0.03, 0.05, 0.07, and 0.10) and the corresponding fitted curves.

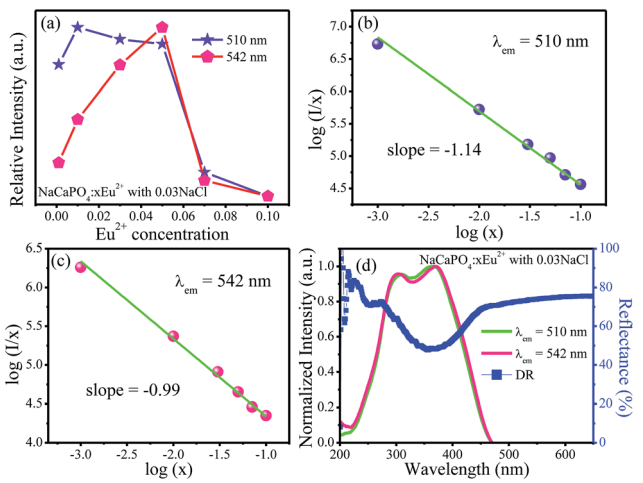

Fig. 9 (a) Variation of emission intensity for $NaCaPO_4$:xEu^{2+} with 0.03NaCl as a function of doped Eu^{2+} concentration. (b) and (c) The relationship of log(I/x) *versus* log(x). (d) DR, excitation spectra, and fitted curves of $NaCaPO_4$:0.01Eu^{2+} with 0.03NaCl, monitored at 510 and 542 nm.

proportional to the n and r of the sample; hence, Eu^{2+} ions with a higher coordination number generally emit at a higher energy, corresponding to a lower wavelength. As a result, 510 (Eu2) and 542 nm (Eu1) emission bands correspond to Ca(2) (Ca(3)) and Ca(1), respectively.

Fig. 9a shows the emission intensities of 510 (Eu2) and 542 nm (Eu1) as a function of Eu^{2+} contents; it can be observed that their emission intensities gradually increased before reaching the maximum at x = 0.01 for 510 nm emission and x = 0.05 for 542 nm emission, respectively. The emission intensities began to decrease with the increasing concentrations of Eu^{2+} due to the concentration quenching effect, resulting from the non-radiative energy migration among the activator Eu^{2+} ions.

Therefore, to further investigate the process of concentration quenching, the type of interaction among the activator Eu^{2+} ions was calculated by the following equation:[32–35]

$$I/x = K[1 + \beta(x)^{\theta/3}]^{-1} \quad (2)$$

where I and x represent the emission intensity and the concentration of the activator ion, respectively; β and K are the specific constants for a given host crystal and excitation condition, and θ = 3, 6, 8 or 10 denotes the non-radiative energy transfer mechanism of exchange coupling, dipole–dipole, dipole–quadrupole, and quadrupole–quadrupole interactions, respectively. The fitted lines of log(I/x) *versus* log(x) for two emission bands centered at 510 and 542 nm are shown in Fig. 9b and c, respectively. The slopes of two fitted lines for 510 and 542 nm emission bands were −1.14 and −0.99, respectively. Therefore, the values of θ were 3.42 and 2.97, close to 3, implying that the main concentration quenching mechanism of Eu^{2+} ions for both 510 and 542 nm emission bands in $NaCaPO_4$ host were the exchange coupling interactions. Fig. 9d shows the DR and excitation spectra of $NaCaPO_4$:0.01Eu^{2+} with 0.03 NaCl, monitored at 510 and 542 nm. It can be seen that the DR spectrum matched well with the excitation spectra of $NaCaPO_4$:0.01Eu^{2+} with 0.03NaCl. $NaCaPO_4$:0.01Eu^{2+} with 0.03NaCl exhibited a broad absorption band from 200 to 450 nm, which was due to the transition of Eu^{2+} that originated from $4f^7$ ground state to $4f^65d$ excitation state. For the excitation spectra monitored at 510 and 542 nm, the spectral width at 542 nm was larger than that at 510 nm due to emission bands that originate from different Eu^{2+} luminescence centers. To further study the reason for different excitation spectra monitored at 510 and 542 nm, their decay curves were measured, as shown in Fig. 10a and b, respectively. A single exponential was used to fit the decay curves, and the effective lifetimes could be defined as:[36,37]

$$\tau = \frac{\int_0^\infty tI(t)\mathrm{d}t}{\int_0^\infty I(t)\mathrm{d}t} \quad (3)$$

where $I(t)$ is the emission intensity at time t and τ is the decay lifetime. The corresponding lifetimes at 510 and 542 nm for $NaCaPO_4$:xEu^{2+} with 0.03NaCl are shown in Fig. 10a and b, respectively. For example, the lifetimes of $NaCaPO_4$:0.01Eu^{2+} with 0.03NaCl for 510 and 542 nm emission bands were calculated to be 339.01 ns and 320.22 ns, respectively, which implies that two emission bands were attributed to two different Eu^{2+} ion luminescence centers.

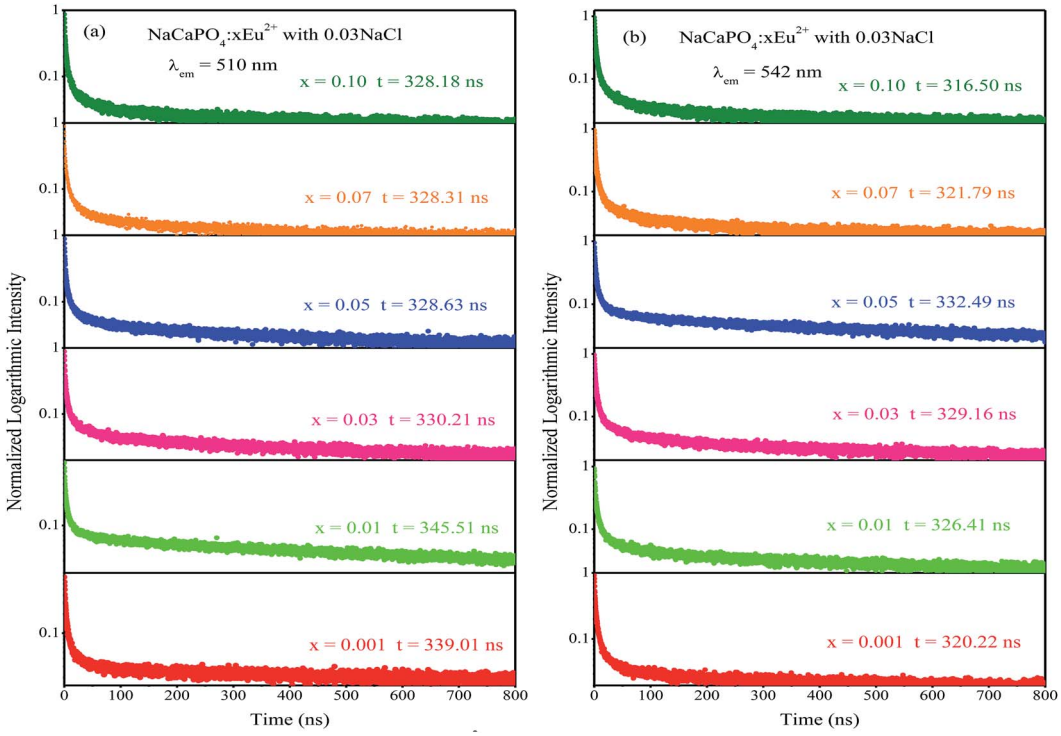

Fig. 10 Decay curves of $NaCaPO_4$:xEu^{2+} with 0.03NaCl monitored at 510 nm (a) and 542 nm (b).

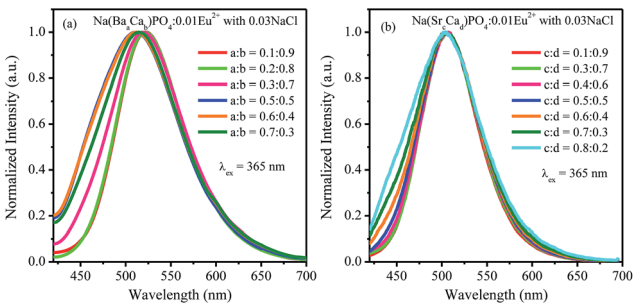

Fig. 11 Normalized emission spectra of $Na(Ba_aCa_b)PO_4$:$0.01Eu^{2+}$ and $Na(Sr_cCa_d)PO_4$:$0.01Eu^{2+}$ with 0.03NaCl excited at 365 nm.

3.2.2.2 $Na(Ba_aCa_b)PO_4$:$0.01Eu^{2+}$ with 0.03NaCl and $Na(Sr_cCa_d)PO_4$:$0.01Eu^{2+}$ with 0.03NaCl. $Na(Ba_aCa_b)PO_4$:$0.01Eu^{2+}$ and $Na(Sr_cCa_d)PO_4$:$0.01Eu^{2+}$ with 0.03NaCl samples were synthesized using a fixed Eu^{2+} concentration of 0.01. The normalized emission spectra of $Na(Ba_aCa_b)PO_4$:$0.01Eu^{2+}$ with 0.03NaCl and $Na(Sr_cCa_d)PO_4$:$0.01Eu^{2+}$ with 0.03NaCl are shown in Fig. 11a and b, respectively, excited at 365 nm. It can be seen that the emission spectra of $Na(Ba_aCa_b)PO_4$:$0.01Eu^{2+}$ with 0.03NaCl show an obvious blue shift with an increase in Ba^{2+} ions. However, when the ratio of Ba and Ca exceeded 0.5 : 0.5, the full width at half maximum decreased. For $Na(Sr_cCa_d)PO_4$:$0.01Eu^{2+}$ with 0.03NaCl, the emission spectra show a broadened full width at half maximum with the increasing Ba^{2+} ions. Based on the abovementioned discussion, the emission spectra could be deconvoluted into two Gaussian components with the maxima at 510 nm (Eu(2)) and 542 nm (Eu(1)). For $Na(Ba_aCa_b)PO_4$:$0.01Eu^{2+}$ with 0.03NaCl and $Na(Sr_cCa_d)PO_4$:$0.01Eu^{2+}$ with 0.03NaCl, the fitted spectra of 510 nm and 542 nm are shown in Fig. 12a–d. The intensities of the 510 nm and 542 nm spectra for $Na(Ba_aCa_b)PO_4$:$0.01Eu^{2+}$ with 0.03NaCl increased with the increasing Ba^{2+} concentration up to $a : b = 0.2 : 0.8$. Due to the concentration quenching effect, the intensities decreased with further increase in the concentration of Ba^{2+} ions. For $Na(Sr_cCa_d)PO_4$:$0.01Eu^{2+}$ with 0.03NaCl, the intensities of 510 nm and

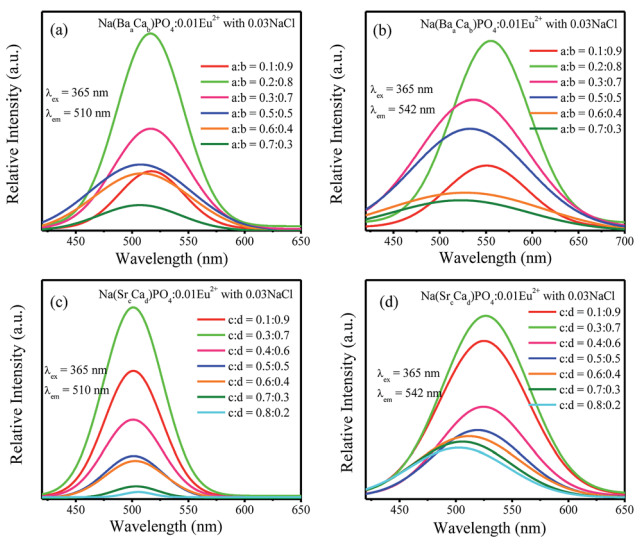

Fig. 12 (a)–(d) Fitted curves at 510 nm and 542 nm for $Na(Ba_aCa_b)PO_4$:$0.01Eu^{2+}$ and $Na(Sr_cCa_d)PO_4$:$0.01Eu^{2+}$ with 0.03NaCl excited at 365 nm.

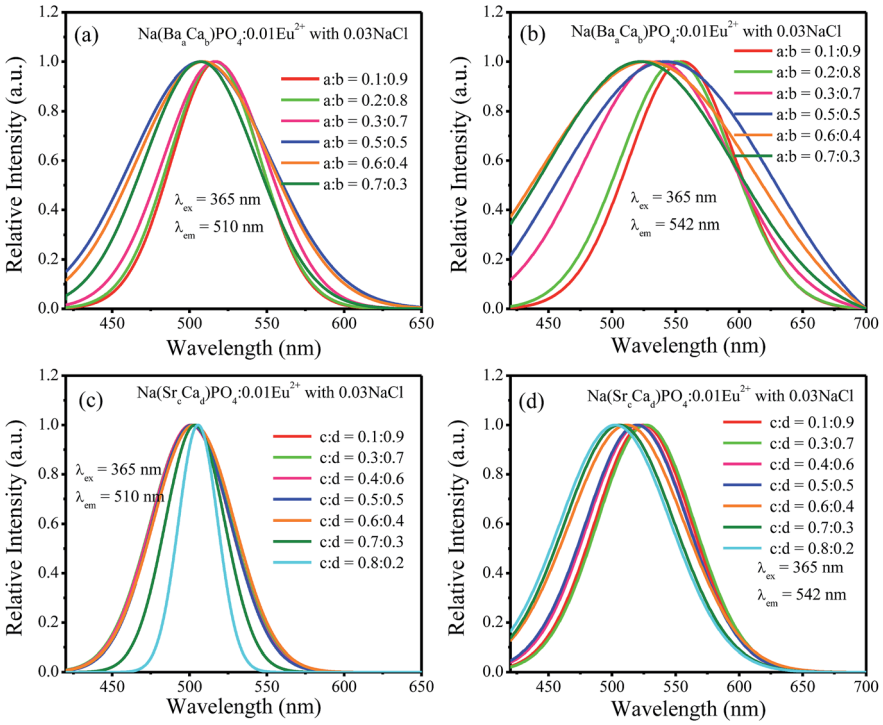

Fig. 13 (a)–(d) Normalized spectra at 510 nm and 542 nm for Na(Ba$_a$Ca$_b$)PO$_4$:0.01Eu^{2+} with 0.03NaCl and Na(Sr$_c$Ca$_d$)PO$_4$:0.01Eu^{2+} with 0.03NaCl excited at 365 nm.

542 nm increased and reached maxima at $c : d = 0.3 : 0.7$ and then decreased with the increment of Sr^{2+} ions concentration. Fig. 13a–d show the normalized spectra of 510 nm and 542 nm for Na(Ba$_a$Ca$_b$)PO$_4$:0.01Eu^{2+} with 0.03NaCl and Na(Sr$_c$Ca$_d$)PO$_4$:0.01Eu^{2+} with 0.03NaCl excited at 365 nm. For Na(Ba$_a$Ca$_b$)PO$_4$:0.01Eu^{2+} with 0.03NaCl, it can be seen that the spectra of 510 nm and 542 nm shifted to a lower wavelength, as shown in Fig. 13a and b, respectively. Moreover, the full width at half maximum of the 510 nm spectra for Na(Ba$_a$Ca$_b$)PO$_4$:0.01Eu^{2+} with 0.03NaCl decreased when the ratio of Ba to Ca exceeded 0.5 : 0.5. However, for Na(Sr$_c$Ca$_d$)PO$_4$:0.01Eu^{2+} with 0.03NaCl, the full width at half maximum of 510 nm spectra decreased when the radio of Sr and Ca was greater than 0.7 : 0.3, and no shift could be observed. The 542 nm spectra showed a blue shift

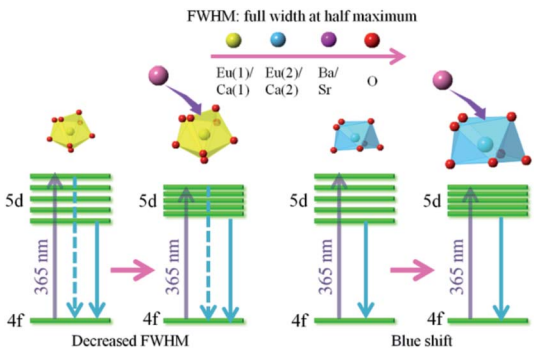

Fig. 14 Schematic of the mechanism accounting for the decreased full width at half maximum and blue shift of Eu^{2+} emission.

with the increase of Sr^{2+} ions. Generally, the crystal field splitting (D_q) trends with bond length can be determined by the following equation:[38–40]

$$D_q = Ze^2r^4/6R^5 \quad (4)$$

where D_q is the magnitude of the 5d energy level separation, Z represents the anion charge or valence, e is the electron charge, r is the radius of the d wave function, and R is the bond length. The bond length of Ce–O will increase due to the lattice expansion because the radii of Ba^{2+} and Sr^{2+} are larger than that of Ca^{2+}. Hence, the crystal field splitting will become weaker, which causes a blue shift and decreases full width at half maximum. The schematic mechanism of the decreased full width at half maximum and blue shift of Eu^{2+} emission is shown in Fig. 14 when Ba^{2+} and Sr^{2+} were substituted for Ca^{2+} in NaCaPO$_4$:0.01Eu^{2+} with 0.03NaCl. The blue shift of Na(Ba$_a$Ca$_b$)PO$_4$:0.01Eu^{2+} with 0.03 NaCl was greater than that of Na(Sr$_c$Ca$_d$)PO$_4$:0.01Eu^{2+} with 0.03NaCl, which is due to that fact that the radius of Ba^{2+} ($r_{Ba} = 1.34$ nm) is larger than that of Sr^{2+} ($r_{Sr} = 1.12$ nm). The crystal field splitting of Na(Ba$_a$Ca$_b$)PO$_4$:0.01Eu^{2+} with 0.03NaCl was weaker, and a more obvious blue shift could be observed. For Na(Sr$_c$Ca$_d$)PO$_4$:0.01Eu^{2+} with 0.03NaCl, comparing the decreased full width at half maximum of the 510 nm band and the blue shift of the 542 nm band, the difference may be that Eu^{2+} had different coordinations (*i.e.*, eight and seven coordination). Therefore, the emission properties could be tuned by controlling the concentration of Ba^{2+} or Sr^{2+}. Fig. 15a and b show CIE chromaticity coordinates and images of Na(Ba$_a$Ca$_b$)PO$_4$:0.01Eu^{2+} with 0.03NaCl and

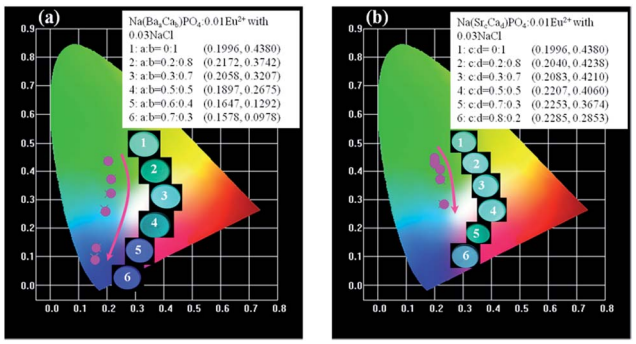

Fig. 15 CIE chromaticity coordinates and images of Na(Ba$_a$Ca$_b$)PO$_4$:0.01Eu^{2+} with 0.03NaCl (a) and Na(Sr$_c$Ca$_d$)PO$_4$:0.01Eu^{2+} with 0.03NaCl (b) under a 365 nm UV lamp.

Na(Sr$_c$Ca$_d$)PO$_4$:0.01Eu^{2+} with 0.03NaCl under a 365 nm UV lamp. It can be seen that the emission color of Na(Ba$_a$Ca$_b$)PO$_4$:0.01Eu^{2+} with 0.03NaCl and Na(Sr$_c$Ca$_d$)PO$_4$:0.01Eu^{2+} with 0.03NaCl could change from green (0.1996, 0.4380) to blue (0.1578, 0.0978) or to cyan (0.2285, 0.2853), respectively. The corresponding images of the samples are shown in Fig. 15.

For LED applications, the thermal stability of the phosphor is one of the important parameters. The temperature-dependent emission spectra of Na(Ba$_{0.7}$Ca$_{0.3}$)PO$_4$:0.01Eu^{2+} with 0.03NaCl and Na(Sr$_{0.8}$Ca$_{0.2}$)PO$_4$:0.01Eu^{2+} with 0.03NaCl under the excitation of 365 nm were investigated, as shown in Fig. 16a and b, respectively. It was observed that the emission intensity continuously decreased with the increasing temperature from room temperature to 200 °C. The emission intensity of Na(Ba$_{0.7}$Ca$_{0.3}$)PO$_4$:0.01Eu^{2+} with 0.03NaCl and Na(Sr$_{0.8}$Ca$_{0.2}$)PO$_4$:0.01Eu^{2+} with 0.03NaCl decreased to 90% and 76% of the initial emission intensity, respectively, corresponding to 100 °C. It can be seen that the thermal quenching of Na(Sr$_{0.8}$Ca$_{0.2}$)PO$_4$:0.01Eu^{2+} with 0.03NaCl was inferior to that of Na(Ba$_{0.7}$Ca$_{0.3}$)PO$_4$:0.01Eu^{2+} with 0.03NaCl. The reason is that in Na(Ba/Sr/Ca)PO$_4$:Eu^{2+} with NaCl, with the replacement of Eu^{2+}–Eu^{2+} neighbors by Eu^{2+}–Ba^{2+}/Sr^{2+} pairs, the emission intensity will decrease with an increment in temperature due to the lower nonradiative decay rate from the lowest excited state, according to Peng *et al.*[41] The bond length will become shorter when Ba^{2+} is co-doped in NaCaPO$_4$:Eu^{2+} with NaCl with respect to Sr^{2+} co-doping because the radius of Ba^{2+} is larger than that of Sr^{2+}. The thermal excitation from Eu^{2+}–Ba^{2+}/Sr^{2+} may occur differently with an increase in temperature. Hence, co-doping Sr will lead to worse thermal quenching compared to co-doping Ba due to covalent effects. The slightly decreased intensity indicated that the Na(Ba/Sr/Ca)PO$_4$:0.01Eu^{2+} with 0.03NaCl phosphor could be applied to a white LED. To investigate the relationship of luminescence with temperature and to calculate the activation energy from thermal quenching, the activation energy (E_a) can be expressed by the following formula:[42]

$$I = I_0/[1 + c\exp(-E_a/kT)] \quad (5)$$

where I and I_0 are the luminescence intensities of the phosphor at the testing temperature and room temperature, respectively, E_a represents the thermal quenching activation energy of the phosphor, c is the rate constant for thermally activated escape, and k is the Boltzmann constant (8.629×10^{-5} eV K^{-1}). The inset of Fig. 16a and b show the plots of $\ln[(I_0/I) - 1]$ *versus* $1/T$ for Na(Ba$_{0.7}$Ca$_{0.3}$)PO$_4$:0.01Eu^{2+} with 0.03NaCl and Na(Sr$_{0.8}$Ca$_{0.2}$)PO$_4$:0.01Eu^{2+} with 0.03NaCl, respectively. The calculated E_a were 0.1506 and 0.2399 eV for Na(Ba$_{0.7}$Ca$_{0.3}$)PO$_4$:0.01Eu^{2+} with 0.03NaCl and Na(Sr$_{0.8}$Ca$_{0.2}$)PO$_4$:0.01Eu^{2+} with 0.03NaCl, which indicate that the phosphors show relatively good thermal stability and can be used in an LED.

To verify the actual application of the phosphor, we chose the sample with the broadest full width at half maximum to fabricate

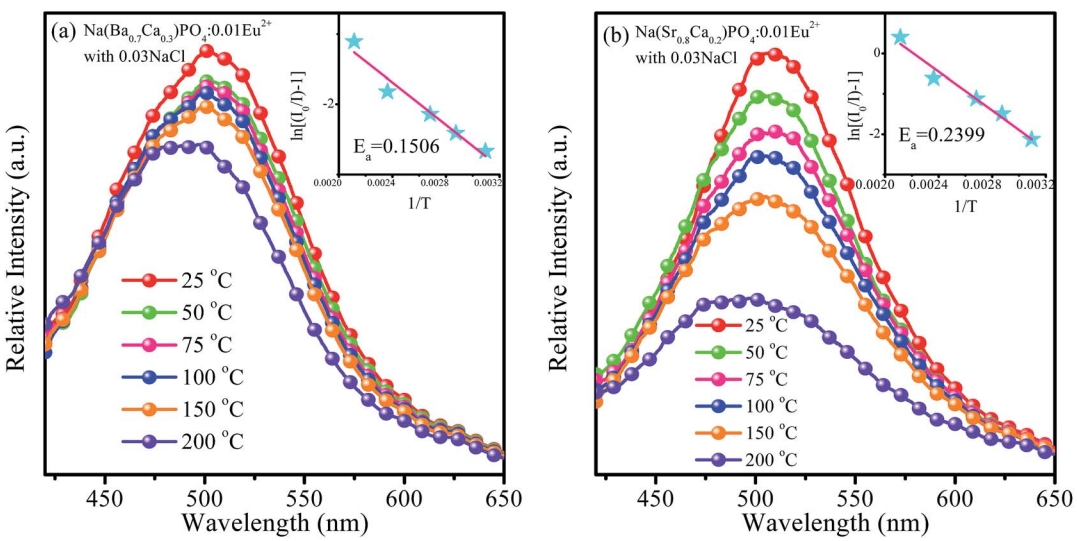

Fig. 16 Temperature-dependent emission spectra of Na(Ba$_{0.7}$Ca$_{0.3}$)PO$_4$:0.01Eu^{2+} with 0.03NaCl (a) and Na(Sr$_{0.8}$Ca$_{0.2}$)PO$_4$:0.01Eu^{2+} with 0.03NaCl (b) excited at 365 nm. The inset shows the activation energy of Na(Ba$_{0.7}$Ca$_{0.3}$)PO$_4$:0.01Eu^{2+} with 0.03NaCl (a) and Na(Sr$_{0.8}$Ca$_{0.2}$)PO$_4$:0.01Eu^{2+} with 0.03NaCl (b).

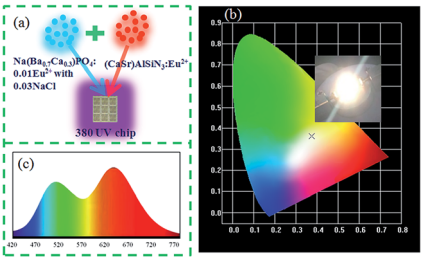

Fig. 17 (a) Diagram of white LED package. (b) CIE chromaticity coordinates and photos of white LED, which is fabricated by $Na(Ba_{0.7}Ca_{0.3})PO_4$:0.01Eu^{2+} with 0.03 NaCl and $(CaSr)AlSiN_3$:Eu^{2+} phosphors. (c) Electroluminescence spectra of white LED composed of a 380 nm UV chip.

a white LED. The devices were combined with a 380 nm UV chip $(CaSr)AlSiN_3$:Eu^{2+} and $Na(Ba_{0.7}Ca_{0.3})PO_4$:0.01Eu^{2+} with 0.03NaCl phosphors, Fig. 17a. CIE coordinates were (0.3750, 0.3634), and the image shows an excellent white light, as shown in Fig. 17b. Fig. 17c shows the electroluminescence spectrum of the white LED. Tt can be seen that the spectrum shows a stronger emission in the range of 480–510 nm. The quantum efficiency of $Na(Ba_{0.7}Ca_{0.3})PO_4$:0.01Eu^{2+} with 0.03NaCl was 45.06%. Therefore, Na(Ba/Sr/Ca)PO_4:0.01Eu^{2+} with 0.03NaCl has potential applications in white LEDs.

4 Conclusions

In summary, a series of Na(Ba/Sr/Ca)PO_4:0.01Eu^{2+} with 0.03NaCl phosphors were synthesized *via* a high-temperature solid-state reaction method. On the one hand, the luminescence intensity of $NaCaPO_4$:Eu^{2+} was enhanced using NaCl as the aid-sintering additives, and the phases were indexed to pure $NaCaPO_4$. $NaCaPO_4$:Eu^{2+} exhibited the strongest emission when the concentration of NaCl was 0.03. $NaCaPO_4$:Eu^{2+} with 0.03NaCl exhibited two green emission bands at 510 and 542 nm, which were ascribed to two different Ca sites with different coordination (*i.e.*, eight and seven coordination). On the other hand, by gradually introducing Ba^{2+} or Sr^{2+} into $NaCaPO_4$:0.01Eu^{2+} with 0.03NaCl, 510 and 542 nm emission bands showed various full width at half maximum and a blue shift caused by the crystal field splitting. The intensity of cyan region from 480 to 510 nm increased by controlling the Ba or Sr concentration. Compared to a Sr^{2+}-doped phosphor, Na(BaCa)PO_4:0.01Eu^{2+} with 0.03NaCl exhibited a more obvious blue shift because the radius of Ba^{2+} is larger than that of Sr^{2+}. Therefore, luminescence of Na(Ba/Sr/Ca)PO_4:0.01Eu^{2+} with 0.03NaCl could be tuned from green (0.1996, 0.4380) to blue (0.1578, 0.0978) under the same excitation by introducing Sr^{2+} or Ba^{2+} ions. Moreover, these phosphors can be used in UV/n-UV-pumped white LEDs.

Acknowledgements

The work was supported by the National Natural Science Foundation of China (No. 51672066), the Funds for Distinguished Young Scientists of Hebei Province, China (No. A2015201129), the personnel training project of Hebei Province, China (No. A2016002013), and the Post-graduate's Innovation Fund Project of Hebei University (No. X2016063, X2016064).

References

1 H. Ji, L. Wang, M. S. Molokeev, N. Hirosaki, R. Xie, Z. Huang, Z. Xia, O. M. Kate, L. Liu and V. V. Atuchin, *J. Mater. Chem. C*, 2016, **4**, 6855–6863.
2 F. Kang, H. Zhang, L. Wondraczek, X. Yang, Y. Zhang, D. Y. Lei and M. Peng, *Chem. Mater.*, 2016, **28**, 2692–2703.
3 S.-P. Lee, S.-D. Liu, T.-S. Chan and T.-M. Chen, *ACS Appl. Mater. Interfaces*, 2016, **8**, 9218–9223.
4 X. Y. Liu, H. Guo, Y. Liu, S. Ye, M. Y. Peng and Q. Y. Zhang, *J. Mater. Chem. C*, 2016, **4**, 2506–2512.
5 H. C. Yoon, H. Kang, S. Lee, J. H. Oh, H. Yang and Y. R. Do, *ACS Appl. Mater. Interfaces*, 2016, **8**, 18189–18200.
6 L. Wang, B. K. Moon, S. H. Park, J. H. Kim, J. Shi, K. H. Kim and J. H. Jeong, *RSC Adv.*, 2016, **6**, 79317–79324.
7 F. Pan, M. Zhou, J. Zhang, X. Zhang, J. Wang, L. Huang, X. Kuang and M. Wu, *J. Mater. Chem. C*, 2016, **4**, 5671–5678.
8 A. A. Setlur, W. J. Heward, Y. Gao, A. M. Srivastava, R. G. Chandran and M. V. Shankar, *Chem. Mater.*, 2006, **18**, 3314–3322.
9 X. Piao, T. Horikawa, H. Hanzawa and K. I. Machida, *Appl. Phys. Lett.*, 2006, **88**, 161908.
10 X. Gong, J. Huang, Y. Chen, Y. Lin, Z. Luo and Y. Huang, *Inorg. Chem.*, 2014, **53**, 6607–6614.
11 K. Li, Y. Zhang, X. Li, M. Shang, H. Lian and J. Lin, *Phys. Chem. Chem. Phys.*, 2015, **17**, 4283–4292.
12 H. S. Jang, W. B. Im, D. C. Lee, D. Y. Jeon and S. S. Kim, *J. Lumin.*, 2007, **126**, 371–377.
13 Y. Zhang, X. Li, K. Li, H. Lian, M. Shang and J. Lin, *ACS Appl. Mater. Interfaces*, 2015, **7**, 2715–2725.
14 D. Wen, J. Feng, J. Li, J. Shi, M. Wu and Q. Su, *J. Mater. Chem. C*, 2015, **3**, 2107–2114.
15 L. Jiang, R. Pang, D. Li, W. Sun, Y. Jia, H. Li, J. Fu, C. Li and S. Zhang, *Dalton Trans.*, 2015, **44**, 17241–17250.
16 C. C. Lin, Z. R. Xiao, G.-Y. Guo, T.-S. Chan and R.-S. Liu, *J. Am. Chem. Soc.*, 2010, **132**, 3020–3028.
17 M.-H. Fang, C. Ni, X. Zhang, Y.-T. Tsai, S. Mahlik, A. Lazarowska, M. Grinberg, H.-S. Sheu, J.-F. Lee, B.-M. Cheng and R.-S. Liu, *ACS Appl. Mater. Interfaces*, 2016, **8**, 30677–30682.
18 F. Kang, M. Peng, D. Y. Lei and Q. Zhang, *Chem. Mater.*, 2016, **28**, 7807–7815.
19 W. L. Wanmaker and H. L. Spier, *J. Electrochem. Soc.*, 1962, **109**, 109–114.
20 M. S. Waite, *J. Electrochem. Soc.*, 1974, **121**, 1122–1123.
21 W. L. Wanmaker, A. Bril and J. W. ter Vrugt, *Appl. Phys. Lett.*, 1966, **8**, 260–261.
22 C. S. Liang, H. Eckert, T. E. Gier and G. D. Stucky, *Chem. Mater.*, 1993, **5**, 597–603.
23 Z. C. Wu, J. X. Shi, M. L. Gong, J. Wang and Q. Su, *Mater. Chem. Phys.*, 2007, **103**, 415–418.
24 Z. C. Wu, J. X. Shi, J. Wang, M. L. Gong and Q. Su, *J. Solid State Chem.*, 2006, **179**, 2356–2360.

25 Y. S. Tang, S. F. Hu, C. C. Lin, N. C. BagKar and R. S. Liu, *Appl. Phys. Lett.*, 2007, **90**, 151108.
26 Z. P. Yang, G. W. Yang, S. L. Wang, J. Tian, X. N. Li, Q. L. Guo and G. S. Fu, *Mater. Lett.*, 2008, **62**, 1884–1886.
27 Y. Wang, M. G. Brik, P. Dorenbos, Y. Huang, Y. Tao and H. Liang, *J. Phys. Chem. C*, 2014, **118**, 7002–7009.
28 C. Larson and R. B. Von Dreele, *Los Alamos National Laboratory Report LAUR*, Los Alamos National Laboratory, Los Alamos, 2000, vol. 86, pp. 748–789.
29 W. Tang and Z. Zhang, *J. Mater. Chem. C*, 2015, **3**, 5339–5346.
30 X. J. Wang, L. Wang, T. Takeda, S. Funahashi, T. Suehiro, N. Hirosaki and R. Xie, *Chem. Mater.*, 2015, **27**, 7689–7697.
31 L. G. Van Uitert, *J. Lumin.*, 1984, **29**, 1–9.
32 L. Ozawa and P. M. Jaffe, *J. Electrochem. Soc.*, 1971, **118**, 1678–1679.
33 L. G. Van Uitert, *J. Electrochem. Soc.*, 1967, **114**, 1048–1053.
34 C. Huang, Y. Chiu, Y. Yeh, T. Chan and T. Chen, *ACS Appl. Mater. Interfaces*, 2012, **4**, 6661–6668.
35 B. Wang, H. Lin, J. Xu, H. Chen and Y. Wang, *ACS Appl. Mater. Interfaces*, 2014, **6**, 22905–22913.
36 Y. Jia, H. Qiao, Y. Zheng, N. Guo and H. You, *Phys. Chem. Chem. Phys.*, 2012, **14**, 3537–3542.
37 Y. Shimomura, T. Honma, M. Shigeiwa, T. Akai, K. Okamoto and N. Kijima, *J. Electrochem. Soc.*, 2007, **154**, J35–J38.
38 C. K. Jorgensen, *Modern Aspects of Ligand-Field Theory*, Amsterdam, North-Holland, 1971.
39 M. Shang, J. Fan, H. Lian, Y. Zhang, D. Geng and J. Lin, *Inorg. Chem.*, 2014, **53**, 7748–7755.
40 Y. Xia, J. Chen, Y. Liu, M. S. Molokeev, M. Guan, Z. Huang and M. Fang, *Dalton Trans.*, 2016, **45**, 1007–1015.
41 M. Peng, X. Yin, P. A. Tanner, M. G. Brik and P. Li, *Chem. Mater.*, 2015, **27**, 2938–2945.
42 S. Bhushan and M. V. Chukichev, *J. Mater. Sci. Lett.*, 1988, **74**, 319–321.